Poda et al., J Nanomater Mol Nanotechnol 2013, 2:1
http://dx.doi.org/10.4172/2324-8777.1000105

Journal of Nanomaterials & Molecular Nanotechnology

Research Article

A SCITECHNOL JOURNAL

Nano-Aluminum Thermite Formulations: Characterizing the Fate Properties of a Nanotechnology during Use

Aimee R. Poda[1]*, Robert D. Moser[2], Michael F. Cuddy[1], Zac Doorenbos[3], Brandon J. Lafferty[1], Charles A. Weiss Jr.[2], Ashley Harmon[1], Mark A. Chappell[1] and Jeffery A. Steevens[1]

Abstract

Nanothermites represent an emerging class of highly efficient propellants/explosive materials whose environmental impacts are poorly understood. In this work, several nanothermite formulations (e.g., Fe_2O_3/Al and Bi_2O_3/Al) were investigated following material transformation during end use. Combustion products were analyzed by SEM, EDS, and XRD. These products subsist with unique physical and chemical forms as compared to the original materials. The combustion process results in the formation of inert spinel structures in the case of the iron-based formulations, whereas Bi_2O_3/Al composites react fully, transforming to metallic bismuth and aluminum oxide. These products are largely resistant to wetting and evidence suggests that transport in aqueous environments would be limited. Due to the particle size ranges found, it is speculated that the main transport route for these materials is aerosolization. These data will ultimately establish a baseline for future studies aimed at an accurate determination of the fate of nanothermite formulations after use.

Keywords

Thermite; Nano-Aluminum; Nano-Bismuth; Toxicity; Environmental; Munition

Introduction

Energetic materials are a major constituent of systems used by all branches of the U.S. Department of Defense (DoD). These materials are used in various military applications including as explosives, projectiles and rocket propellants. In recent years, researchers have found that nano-sized energetic materials/ingredients incorporated into thermite formulations promise increased performance through a number of desirable properties, including enhanced sensitivity, reaction rate, pressure generation, stability, energy release, and mechanical strength [1]. The burgeoning interest in these engineered nanomaterials necessitates new energetic materials research and development strategies and so offers opportunities for revolutionary enhancements in weapons systems.

In general, thermites are a pyrotechnic composition of a stoichiometric mixture of metal powder and a metal oxide that produces an exothermic oxidation-reduction reaction known as a thermite reaction. The heat output from a thermite reaction is determined by the free energy change associated with reduction of the oxide and simultaneous oxidation of the metal [2]. The thermite reaction employed in many military applications is the reaction of a stoichiometric mixture of micron-sized Al metal and magnetite (Fe_3O_4) reacting exothermically to completion to produce alumina (Al_2O_3) and iron. Many other thermite mixtures exist [3]. The reactant composition can be chosen to produce solid, liquid, and/or gaseous products as required for the particular application. For military engineering applications, the optimal thermite mixture is dependent on several factors that include the energy per unit mass, chemical stability, chemical compatibility, availability, processing ease, cost and the toxicity of the reactants and products [4].

One important design point in manipulating the rate of energy release involves selecting the particle sizes of metal/metal oxide components [1]. Historically, pyrotechnic or explosive applications for bulk scale thermites have been limited due to their relatively slow energy release rates. But, because nanothermites are created from reactant particles with proximities approaching the atomic scale, energy release rates are greatly improved [5]. Traditional thermite reactions utilizing micron-sized Al powder feature long ignition delays, slow burning rates, and incomplete combustion [6]. Nanothermites have generated great interest in the last decade due to their superior thermodynamics properties. The advantage of nanoenergetic materials is that they can release stored energy much more rapidly as compared to conventional energetic materials. The energy release can be tailored so as to maximize the effect of nanoenergetics-based applications, such as in projectiles or airbag initiators. Recent developments of nanoscale energetic materials research have leveraged new and technologically useful characteristics of nanoreactants leading to enhanced reactivity based on a significant increase in the specific surface area [7-11]. Due to the small particle size and large surface area of nanoreactants, the number of contact points is greatly increased over traditional thermite materials leading to more efficient combustion. Energy release rates for nanothermites are increased due to short diffusion paths of reactants; as such, overall reaction rates can surpass those of traditional thermite reactions by several orders of magnitude [12]. Recently, Wang et al. [13] showed that nano-sized Al particles generate the peak pressure associated with the thermite reaction ~10^4 times faster than micron-sized reactants.

The advances in engineered nanomaterials have outpaced environmental, health, and safety (EHS) research, resulting in a growing divide between product development and safety. Although research efforts have been made to examine the potential environmental impact of nanomaterials [14], many of these studies focused on pristine systems, each with unique physical characteristics requiring examination with a multitude of exposure scenarios. In reality, product residues resulting from transformations caused by product incorporation and from direct use are much more relevant for toxicological studies and risk assessment than pristine nanomaterials. The risks associated with exposure to nanomaterials require knowledge about the composition, physical nature, and the processes that control their environmental fate and transformations [15].

***Corresponding author:** Aimee R. Poda, PhD, Environmental Laboratory, US Army Engineer Research and Development Center, 3909 Halls Ferry Rd., Vicksburg, MS, 39180, USA, Tel: 1 601 634 4003; E-mail: Aimee.R.Poda@usace.army.mil

Received: November 15, 2012 **Accepted:** January 04, 2013 **Published:** January 09, 2013

The goal of this study is to answer the question: what is the state of the spent nanothermite material after use? In collaboration with the developers of this technology, four different nanothermite formulations containing nano-sized metal/metal oxide particles were characterized following nanopowder product incorporation and controlled combustion tests. The physical and chemical properties (i.e., size, composition, morphology) of the spent material and also parameters that describe its fate (i.e., adsorption of water on surface of particles, dissolution of particles, and settling properties of particles in water) were extrapolated to gauge potential for exposure to these products. These physical property data lay the foundation for follow-on studies related to risk, environmental fate and toxicological impacts of nanothermite residues.

Materials and Methods

Materials acquisition

Four energetic residues provided by Innovative Materials and Processes, LLC (IMP) were examined in this study. Table 1 details the original material starting compositions and the material suppliers of the pre-ignited material. This table also introduces the naming convention for the material residues that will be discussed throughout this manuscript. IMP disclosed that four of the raw materials were obtained from commercial suppliers while the nanoscale flake (Table 1) was a proprietary material produced by the company. Three of the residues were composed of mixtures of Bi_2O_3 and Al with similar initial material compositions. One of the residues (Sample 1) was a Fe_2O_3 and Al mixture with a higher percentage of Al as compared to the Bi-based formulations. More information on material composition and material performance can be found in the literature [6,12,16-18].

Scanning electron microscopy (SEM) and transmission electron microscopy (TEM) were employed to generate representative images of the raw materials (Figure 1). These images show the variation in particle size and illustrate the material shape prior to compounding and combustion. The Nova Centrix Al shown in figure 1A was about 80 nm in size and existed as agglomerated particles as imaged with SEM. These Al nanoparticles were synthesized using a high power (50-100 MW), pulsed electrical arc discharge between two feedstock metal rods [19]. Representative particles of an Al flake material with flakes ranging in size from the micron range to the nanoscale and thickness of <500 nm produced by IMP are shown in figure 1B. As characterized by the supplier, the Accumet Bi_2O_3 CAS# 1304-76-3 was 99.9% pure with an average particle size of 85-128 nm [20]. This material was spherical and had an average surface area of 3-4 m^2/g (Figure 1C). Clark Bi_2O_3 CAS# 1304-76-3 is shown in figure 1D. The reported surface area was 0.8-1.0 m^2/g with a particle distribution ranging from nanometer-sized particles to particles exceeding 5

Table 1: Pre-ignited thermite material nominal composition (mass %), size, and manufacturer for samples examined in this study.

Sample ID	Al [80 nm] (NovaCentrix)	Bi_2O_3 [3-4 m^2/g] (Accument)	Fe_2O_3 (Nano Amor)	Bi_2O_3 [0.8-1 m^2/g] (Clark)	Al, nanoscale flake [24 m^2/g] (IMP)	Misc. Fillers
Sample 1	29.3%		67.5%			3.2%
Sample 2				84.7%	12.6%	2.7%
Sample 3	12.6%	84.7%				2.7%
Sample 4	12.6%			84.7%		2.7%

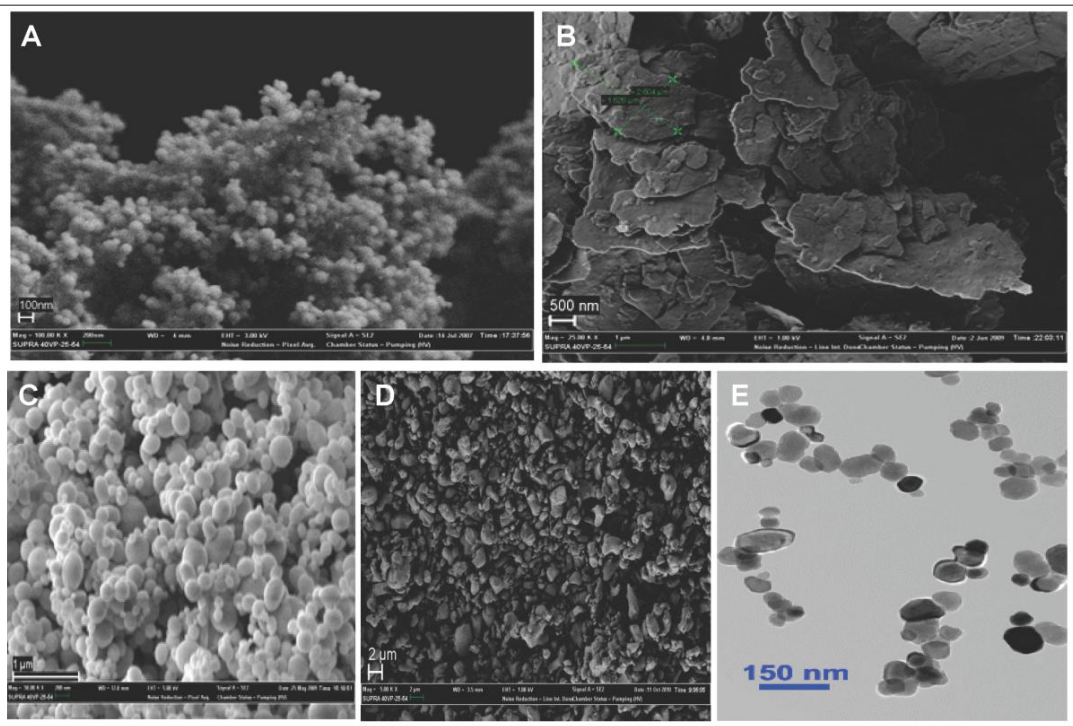

Figure 1: Representative SEM images of the thermite materials prior to reaction. (A) 80 nm Al particles (NovaCentrix), (B) Al flakes (IMP), (C) Bi_2O_3 spheroid particles (Accumet), and (D) Bi_2O_3 spheroid particles (Clark). Transmission electron micrograph (E) is shown for α-Fe_2O_3 (NanoAmor).

microns with a purity exceeding 99% [21]. Figure 1E shows a TEM image of the Fe_2O_3 (alpha) from Nanostructured and Amorphous Materials (NanoAmor). This material was reported as 98% pure with an average particle size of 20-60 nm and a specific surface area of 20-60 m^2/g [22].

Energetic compounding

Prior to ignition, the raw materials were compounded by IMP to produce the nanothermite mixtures. These powders were mixed according to the water-based mixing method of Puszynski et al. [23]. The thermite formulations were prepared using a one-step mixing process in a Resodyn LabRAM mixer as opposed to typical ultrasonication. The nanothermite materials were formulated according to the stoichiometric ratios of fuel (i.e., Al NPs) and oxidizer (X_2O_3, X=Fe, Bi) with the aid of ammonium dihydrogen phosphate to protect the aluminum from oxidation, and 2.4 wt% Arabic gum as a binder. After mixing, the material was dried in flowing air for 2 hours and then stored in a desiccator for a minimum of 12 hours before combustion experiments were conducted.

Residue Generation (Ignition/Combustion Process)

The nanothermite residue samples were prepared by the combustion of the compounded nanothermite mixtures. Combustion was performed in a 300 cm^3 closed bomb with varying amounts of thermite mixtures (0.5 to 2 g). The atmosphere within the closed bomb was air and the combustions were carried out under ambient conditions of temperature and pressure. The samples were ignited using a 32-gauge NiCr wire with power supplied by a 12 V, 10 A battery. The temperature and peak pressure during the combustion event ostensibly achieve those of the adiabatic values well documented in the literature [3]. After combustion, the residue was scraped from the closed bomb and collected. This process was repeated for each of the thermite mixtures, and several repetitions were performed to provide enough residues for testing. The collection efficiency of the residue ranged from 75 to 90 % recovery compared to the original pre-combustion mass. These high recovery values are credited to the increased condensation of the combustion products in the closed bomb configuration.

Physical and chemical properties

Particle size analysis: Spent residues included in the study were analyzed to determine their particle-size distribution at two different length scales. First, the as-received material was filtered through a series of sieves to determine the approximate particle-size distribution. Residue fractions below 75 µm and greater than 75 µm, 425 µm, and 850 µm were collected, and the weight percent of each sieved fraction was determined. The proportion of small particles in the residue (i.e., the fraction < 75 µm) were then further analyzed using quantitative image analysis techniques (Image Pro Plus) in conjunction with SEM micrographs.

X-ray Diffraction: The mineralogy of each spent residue was determined using X-ray diffraction patterns obtained using a Panalytical X'Pert Pro diffractometer using a Co-Kα source operating at 45 kV and 40 mA. Diffraction patterns were obtained from 2-80°(2θ) with a step size of 0.002°(2θ) and total scan time of 3 hr. Qualitative phase identification was performed using Jade 2010 (MDI) and X'Pert High Score (Panalytical) analysis software.

Scanning electron microscopy/energy-dispersive x-ray spectroscopy: The morphology and elemental composition and distribution in chemistry of the spent residues were determined using SEM along with energy-dispersive X-ray spectroscopy (EDS). Backscattered scanning electron micrographs were obtained using an FEI Nova NanoSEM 630 field-emission SEM operated at 5 kV. EDS elemental maps were obtained using an integral Bruker AXS Quantax microanalysis system with the electron beam operating at 15 kV. Bulk elemental compositions of the sieved nanothermite residues were determined using a Shimadzu EDX-800HS energy dispersive X-ray fluorescence spectrometer (EDX) equipped with a liquid nitrogen cooled Si(Li) detector and Rh anode as the X-ray source. 10 mm of each sample was exposed to X-rays under an evacuated atmosphere (30 Pa), and data were collected for 100 seconds for each sample.

Fate parameters

Dissolution screening: A modified EPA Method 1312 (Synthetic Precipitation Leaching Procedure) was used for the dissolution screening experiments. Dissolution measurements were performed in triplicate using test tubes containing 50 mg of spent residue with 2.0 ml of Milli-Q (18 MΩ-cm) water, acid rain leachate, or moderately-hard reconstituted water (MHW) and mixed on a shaker bath for 14 days. A 1.0 ml sample was extracted from each test tube at the 14-day time point, filtered through a 0.45 µm syringe filter and finally diluted with 2.0% HNO_3 to a volume of 4.0 ml prior to analysis.

Analysis of dissolved metals was performed using inductively-coupled plasma atomic emission spectroscopy (ICP-AES) after sample acidification using EPA Method SW-846/6020. The analytical limit of detection for Bi, Fe, and Al was 0.001 mg L^{-1}, and the limit of quantification was 0.002 mg L^{-1}.

Settling study: Post-combustion particles were suspended in dilute electrolyte solution (10 mM $NaNO_3$), and the change in particle concentration due to gravimetric settling was monitored with time. Analyses were conducted in duplicate. Measurements were obtained by recording the change in the suspension turbidity (i.e., attenuation of light through the suspension). This attenuation, representing the exponential decrease of the intensity of light passing through the medium, is described as

$$I_{trans} = I_0 e^{-\tau x} \quad (1)$$

where τ is the turbidity of the medium (cm^{-1}), which is directly related to the number density (N) of individual extinction cross sections (σ_{ext}) as

$$\tau = N\sigma_{ext} \quad (2)$$

where the extinction coefficient $\sigma_{ext} = \sigma_{abs} + \sigma_{scat}$. Assuming $\sigma_{scat} >> \sigma_{abs}$, then τ represents the number density of particles due to light scattering. This was confirmed with preliminary UV-vis spectra so that no particular absorbance was observed for nano Al particles at 600 nm.

TGA/DSC analysis: Thermal analyses including thermogravimetric analysis (TGA) and differential scanning calorimetry (DSC) were utilized to determine the propensity of the residues to physically adsorb water and to identify specific phases based on thermal degradation or phase changes. Thermal analysis measurements were performed on a Netzsch TG 449 F1 Jupiter combined TGA/DSC from 25-1000°C at a temperature ramp rate of 10°C/min.

Results and Discussion

A principal environmental consideration associated with the

release of nanomaterials, either intentionally or inadvertently, is how the material characteristics will dictate its transport, fate, and ultimate exposure to non-target receptors [24]. Little is known about the fate of spent nanothermite materials once they enter the environment. In addition, information is generally lacking that describes physical characteristics after product incorporation and subsequent to utilization. To date, the literature has mainly focused on the synthesis of nanothermite formulations along with ignition and combustion dynamics [25-28]. Here, we attempt to provide insight as to the chemical composition and physical characteristics of spent nanothermite materials after reaction and speculate on the environmental fates of the spent residues based upon various analytical techniques.

Particle sizing was performed to determine if the residue remained in the nano regime post-detonation. In the case of Sample 1, the majority of the residue, 87%, was measured as greater than 75 μm in size. The smallest fraction, 13%, classified as fines, was represented by the collected fraction <75 μm. In contrast, all residues for Samples 2-4 were measured as <75 μm using the sieve method. Representative SEM images of the four spent residues in the <75 μm sieved fraction are shown in figure 2. Sample 1 (Al/Fe_2O_3-based) particles were angular in nature and ranged from nano- to micro-scales in size (Figure 2A). Samples 2, 3, and 4 (Al/Bi_2O_3-based) exhibited similar spherical particle morphologies with diameters of hundreds to thousands of nanometers (Figures 2B-2D). In the case of the Al/Bi_2O_3-based samples, nano-scale particles with lower grayscale (likely lower density as indicated by backscattered SEM imaging) were adsorbed on the surface of the spherical Bi particles. This is depicted in figure 3, where Al_2O_3 particles can be seen adhering to the substantially larger Bi sphere. The image in figure 3 is also representative of the spent residues of Samples 2 and 4. Notably, particles in Al/Fe_2O_3 residues tend to be larger than particles in Al/Bi_2O_3 residues, despite the relatively low boiling point for Bi (~1840 K) and a presumable adiabatic temperature of 3319 K for the thermite reaction. It is speculated that the smaller particles formed in the Al/Bi_2O_3 formulations arise in part due to pressure unloading (the peak pressure of the Al/Bi_2O_3 system has been reported to be significantly greater than that of the Al/Fe_2O_3 system [3]) which causes rapid thermal dissipation and cooling of the product material, ultimately resulting in a reduced propensity for condensation of large particulates. The mechanisms directing this phenomenon, seemingly preferentially in the Al/Bi_2O_3 formulations, are not well understood and represent a good point for future investigations.

In addition to SEM imaging, EDS elemental mapping was used to investigate the spatial distribution in chemical composition of the nanothermite residues. Figure 4A shows an SEM image of a typical particle present in Sample 1 with a corresponding elemental map (Figure 4B). Here, a triple-phase mixture is observed in the backscattered SEM image and elemental map with the small brightest inclusions being primarily iron-based (likely residual Fe_2O_3), the medium grayscale phases being Al, Fe oxides, and the darkest grayscale pertaining primarily to aluminum (likely Al_2O_3). These observations of morphology and chemical composition of the Al/Fe_2O_3-based nanothermite residues when compared with the initial reactants, figure 1, suggests that the reaction of the traditional thermite form, $2Al + Fe_2O_3 \rightarrow 2Fe + Al_2O_3$, effectively transforms the materials, resulting in no remnant structures following the thermite reaction. In addition, the multi-phase structure that is formed likely results from the rapid quenching of the molten reaction product, leading to the formation of high temperature Al, Fe oxides (e.g., spinel structures) that typically have very low solubility compared with the reactants [29,30]. Indeed, the adiabatic temperature for the reaction shown above is 3135 K [16], suggesting that very high temperatures can be achieved in the closed bomb combustion environment. This will be expounded upon in succeeding discussions.

Figure 4 also provides an SEM micrograph (Figure 4C) and corresponding elemental map (Figure 4D) of a typical particle observed in Samples 2-4 (Sample 3 is represented here). Here, the brighter spherical particle consists primarily of elemental Bi. Traces of aluminum corresponded with the nano-scale adsorbed particles with lower grayscale (likely Al_2O_3) on the surface of the Bi spheres (Figure 3). Similar to the Al/Fe_2O_3-based nanothermite residues, the Al/Bi_2O_3-based nanothermites also seem to have

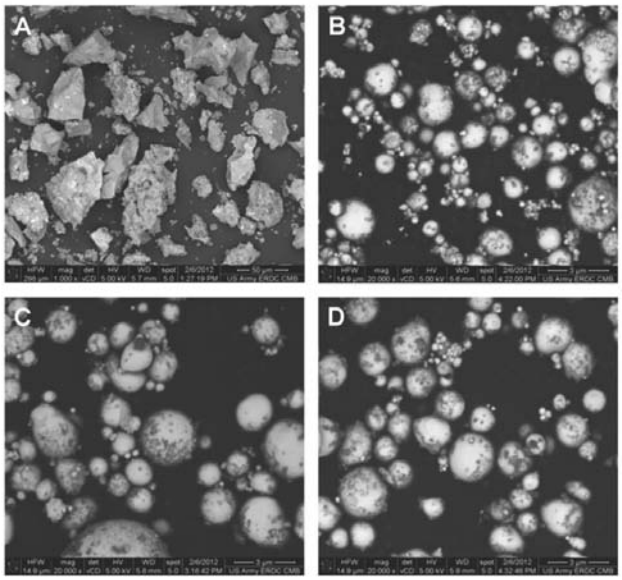

Figure 2: Representative SEM images of thermite materials subsequent to detonation events. Sample 1 (A) images the residual of the thermite made from 80-nm Al particles (NovaCentrix)/20-60 nm Fe_2O_3. Sample 2 (B) images the residual of the thermite made from Al flakes (IMP)/Bi_2O_3 particles (Clark). Sample 3 (C) images the residual of the thermite made from 80-nm Al particles (NovaCentrix)/Bi_2O_3 particles (Accumet) and Sample 4 (D) images the residual of the thermite made from 80-nm Al particles (NovaCentrix)/Bi_2O_3 particles (Clark).

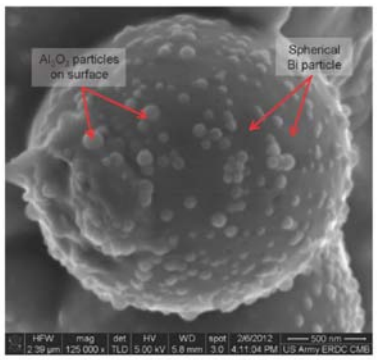

Figure 3: High-resolution SEM image of a typical particle in Sample 3. Main spherical particle composed of elemental Bi with adsorbed Al_2O_3 particles present on the surface.

undergone a full transformation ($2Al + Bi_2O_3 \rightarrow 2Bi + Al_2O_3$, adiabatic temperature=3319 K [16]) during the thermite reaction with no remnant structures present in the residues. Particle morphologies and observed composition suggest partitioning of Al and Bi in the molten state, leading to the formation of spheres of elemental Bi by rapid condensation when suspended in air following the pyrotechnic event, with residual Al oxidizing to nano-scale Al_2O_3 particles.

Investigations of particle size for the spent residues by quantitative image analysis of SEM micrographs showed a general increase in mean particle size of all nanothermites following thermitic reactions. Particles ranged from approximately 100 nm to 50 µm with a mean particle size of ~7 µm in size in Sample 1 (Figure 5A). However, it is clear from the histogram in figure 5A that the greater majority of particles are present in the 100-nm to single-µm size range. Figure 5B shows the particle-size distribution obtained for Al/Bi_2O_3 nanothermite (Samples 2, 3, and 4). The Al/Bi_2O_3-based nanothermites exhibited a much narrower size distribution, with particles ranging in size from 10^2-10^3 nm. The mean particle sizes were 0.72, 0.96, and 0.99 µm for samples 2, 3, and 4, respectively. A portion of nano-sized particles smaller than those represented in the histograms in figure 5B is likely present but could not be fully resolved in the SEM images obtained for the purpose of image analysis.

Bulk chemical analysis results from EDS for all samples are presented in table 2. In the case of the Al/Fe_2O_3-based nanothermite, Sample 1, the residue chemical composition is similar to that of the starting material. However, the Al/Bi_2O_3-based nanothermites, Samples 2, 3, and 4, exhibited a minimal amount of Al in the residues. Indeed, Bi accounted for >90% of the total composition of each residue for these samples. These results, along with the particle morphologies observed in SEM images, suggest that aluminum oxides present in these nanothermites exist as nano-sized particles in the spent residues that may be more readily aerosolized following combustion,

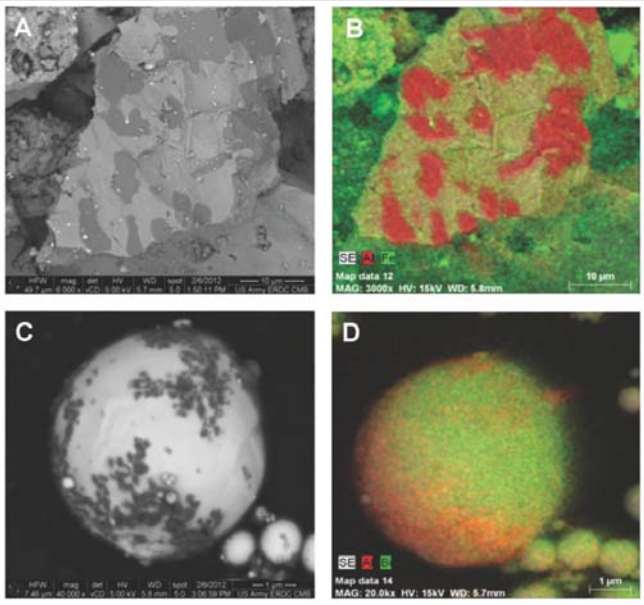

Figure 4: (A) Backscattered SEM micrograph and (B) corresponding EDS map of Al and Fe for Sample 1, showing dual-phase structure with regions that are rich in Al (darker) and regions that are rich in Fe (lighter). Similar images are provided for Sample 3 in (C) and (D), respectively, showing bright regions in the SEM micrograph associated with Bi and darker adsorbed particles associated with Al. (C) and (D) are also representative of Samples 2 and 4.

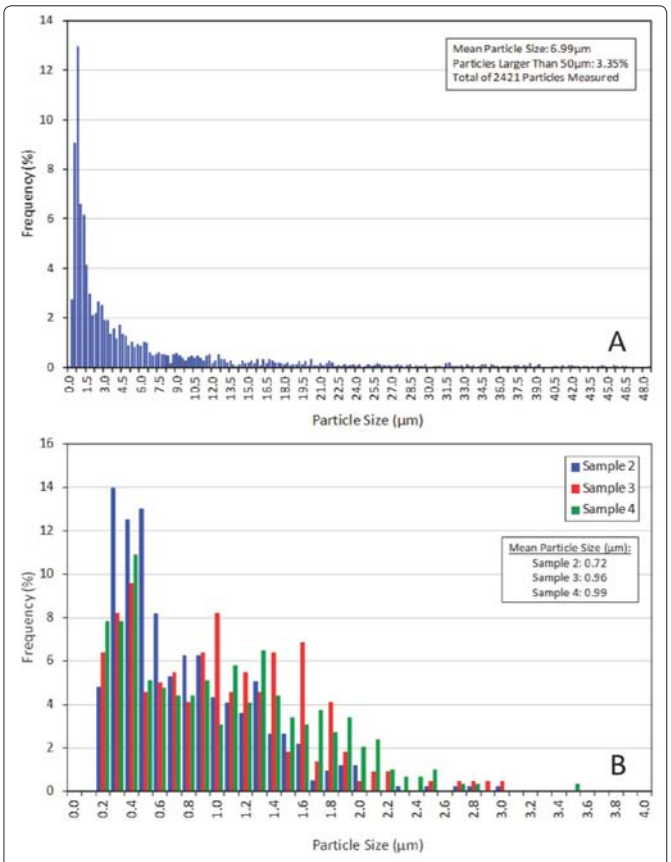

Figure 5: Particle size distributions obtained from image analyses of SEM micrographs. (A) Sample 1 with mean particle size = 6.99 µm. (B) shows particle size distributions for Samples 2 (blue), 3 (red), and 4 (green). Here, the mean particle sizes are 0.72, 0.96, and 0.99 µm for Samples 2, 3, and 4, respectively.

Table 2: Bulk chemistry (mass %, from EDS analyses) for selected elements of post-ignition thermite materials for samples examined in this study.

Element	Sample 1	Sample 2	Sample 3	Sample 4
Bi		98.89	91.27	98.1
Fe	74.78	0.23	1.05	0.128
Al	24.16		5.99	0.919
P	0.69	0.38	1.29	
Ca	0.17	0.49	0.39	0.598
S	0.09			
Cr	0.11			
Ni				0.256
Total	100	100	100	100

assuming these particles are not bound to larger materials released with the residue. The ramifications of this potential aerosolization are discussed below. In addition, the nano Al_2O_3 products may effectively be shadowed by the bulkier Bi matrix, thus inhibiting Al detection by the EDS technique and resulting in the apparent near-total loss of aluminum. This is supported by XRD results that suggest that Al is generally not incorporated into the crystal structure of the particles formed from combustion of the Al/Bi_2O_3-based nanothermites. Moreover, each Al/Bi_2O_3-based sample must retain a significant

Table 3: Total dissolved metal concentration (in ppb) after 14 days in the indicated media.

Sample	Acid Rain Leachate			MHW			Milli-Q Water		
	Al	Bi	Fe	Al	Bi	Fe	Al	Bi	Fe
1	121 ± 19	--	2620 ± 3885	113 ± 18	--	575 ± 302	87 ± 7	--	71 ± 44
2	50 ± 4	116 ± 6	--	236 ± 132	119 ± 45	--	64 ± 1	131 ± 7	--
3	110 ± 74	213 ± 119	--	285 ± 39	119 ± 28	--	73 ± 30	150 ± 56	--
4	138 ± 82	111 ± 6	--	208 ± 111	78 ± 13	--	54 ± 47	97 ± 10	--

concentration of Al in some form, as the dissolution products from these samples (Table 3, discussed below) contain significant portions of dissolved Al. Thus, the values presented in table 2 represent a lower limit on the percent Al present in the spent residues.

Another valuable piece of information regarding the spent residues is the crystal structure of the material. X-ray diffraction analysis was used to determine the phases present in the residual of the thermite materials. The XRD pattern from Sample 1 (Figure 6A) indicates that the resultant phases after combustion are minerals from the spinel family; principally the mineral hercynite (nominally Al_2FeO_4, a spinel product likely induced by the high temperature of the reaction) with minor constituents of corundum (Al_2O_3) and wuestite (FeO). This is not unexpected, as the starting material contains mostly Fe_2O_3 and Al. It does show, however, that a significant portion of Al is sequestered by conversion to the largely insoluble hercynite. The XRD patterns for Samples 2, 3, and 4 (Figure 6B) indicate the presence of elemental Bi with small amounts of corundum (Al_2O_3). Interestingly, Al reactants are not incorporated in a spinel phase in these formulations as compared to Sample 1, where a considerable portion of hercynite was observed. This indicates that the Al/Bi_2O_3, rather than Al/Fe_2O_3, formulations preferentially give rise to a more effective thermite reaction in which the process effectively goes to completion.

It is evident from the particle analysis data that significant differences exist between the Al/Fe_2O_3 and Al/Bi_2O_3 thermitic formulations. These discrepancies have implications for the potential of particle uptake in air and inhalation risks associated with airborne particles. Thus, we have developed conjectures regarding particle uptake based upon the results of our investigations. Limited information is available at this time in regards to particle inhalation hazards associated with these nanothermite formulations in their spent form. Generally, the product materials discussed here are considered relatively non-toxic [31-34]. However, alumina aerosols (speculated to arise from the Al/Bi_2O_3 nanothermite formulations; see above) in particular may demonstrate some toxicity. Warheit et al. [35] and coworkers reported that TiO_2 particles heavily surface-treated with alumina produced adverse pulmonary effects upon inhalation by rats. Moreover, other nanoparticles (carbon nanotubes) have already been shown to directly result in significant mortality, chiefly ascribed to airway blockage, upon inhalation by rodents [36,37]. Inhalation of airborne nanomaterials is a main exposure route for humans [38]. Generally, particles between 2.5 and 10 μm in aerodynamic diameter correspond to the inhalable particles capable of being deposited in the upper respiratory tract, whereas those sized at less than 2.5 μm represent a fine particle that could be capable of penetrating the alveolar region of the lung [39]. Because the majority of the particles in samples 2-4 exist at or below the 2.5 μm cut-off, these materials could pose some threat by inhalation and as such, warrant further investigation.

In addition to considerations with respect to inhalation hazards of potentially airborne materials, it is also important to consider the propensity for the material to be transported through air. The effective span of contamination of spent nanothermite residues will be at least partially attributed to the size of the products. Smaller, lighter particles will remain aloft much longer than bulkier, heavier particles, rendering transport of the material more plausible. This increase in transport could increase the chance of exposure. In the case of Sample 1, the majority of the particles (86.6%) are larger than 75 μm with only a small percentage (13.4%) existing in the <75 μm size range. In this instance, there is less material available for uptake in air as the larger particles are expected to gravity-settle and behave more like bulk material. Despite the potential for transport through air, particle agglomeration or particle adhesion to substrates often limits this transport mode [40]. Thus, it is imperative to also consider the effect of transport through other media (i.e., water or soil) and how these facilitate particle fate. In order to assess the fate parameters associated with the spent materials, various analytical techniques were used to

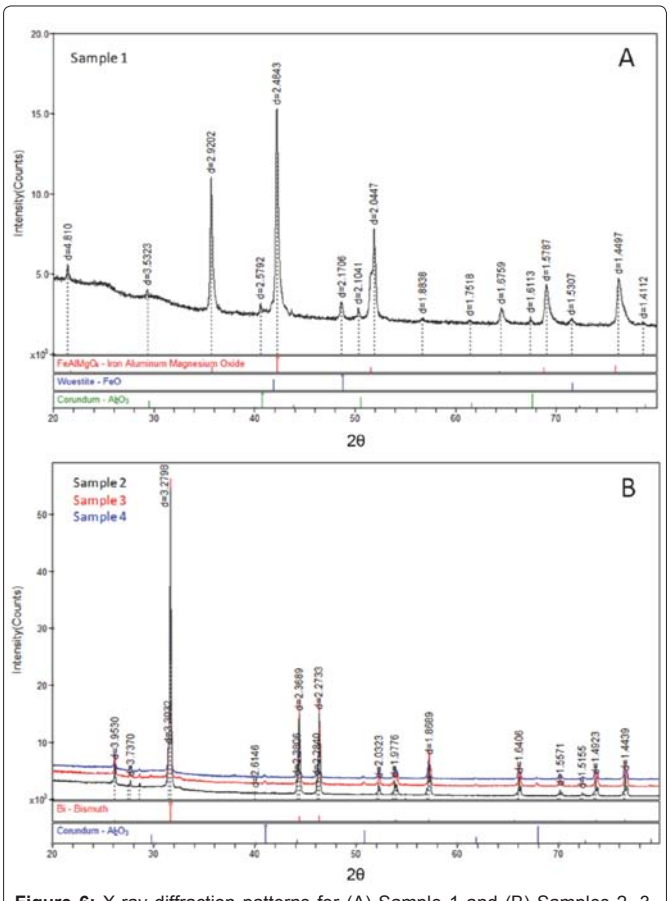

Figure 6: X-ray diffraction patterns for (A) Sample 1 and (B) Samples 2, 3, and 4.

investigate the thermal and wetting properties, dissolution, and water settling in samples 1-4.

Thermal analysis consisted of simultaneous TGA and DSC measurements from 35°C to 1000°C (Figure 7). In all samples, a negligible amount of mass loss (less than 0.2%) was observed up to 105°C, indicating little wetting of the particle surfaces when exposed to ambient relative humidities (samples conditioned at 50% relative humidity). These results suggest that wetting of the particles is inefficient and as such, imply that the sub-micron residues will experience limited mobility in aqueous media [41,42]. In samples 2, 3, and 4, an endothermic peak is centered at 271°C, indicative of the melting event for metallic Bi. The integrated area under the endothermic peak was approximately 38 J/g compared with the heat of fusion of Bi of 51.9 J/g, indicating that the Al/Bi_2O_3-based nanothermite residues are composed of approximately 73% elemental Bi by weight. This is close to the theoretical stoichiometric maximum for production of metallic bismuth of 80.4%, suggesting the reaction $2Al + Bi_2O_3 \rightarrow 2Bi + Al_2O_3$ goes nearly to completion.

Dissolution studies were conducted to determine the relative solubilities of the residues in matrices used for environmental fate and transport or biological toxicity studies. Table 3 lists the metal content in parts per billion for each of the three media, i.e., acid rain leachate, MHW, and Milli-Q water, after a 14-day testing period. Acidification of a water source generally promotes dissolution of nanomaterials [43]; this is reflected in the results depicted in table 3, where dissolved metal content was up to twice as great for acid rain leachate as for Milli-Q water. Generally, the dissolved concentrations of Al in the MHW medium (representative of surface water) were larger than those observed for the other two media, indicating favorable dissolution of Al-based particles in hard water. This observation is not unprecedented, as similar results were reported by Darlington et al. [14]. Nonetheless, they report very limited mobility of the MHW-dissolved Al nanoparticles and attribute this phenomenon to the presence of agglomerated particles in the MHW matrix. The extreme variability in the data for Sample 1 makes commenting on the Fe solubility difficult. As observed with XRD (Figure 6A), Fe exists as a mixed spinel phase that generally has limited solubility [44]. In the case of metallic Bi in samples 2-4, similar dissolution amounts were observed in all three media. In all cases, low dissolution was observed, consistent with the expected low solubility of metallic Bi. Overall, the relatively small dissolved fractions of Al, Bi, or Fe are consistent with the aforementioned XRD data, which show that insoluble spinel phases and/or metallic products dominate the thermitic residues. Accordingly, it should be noted that preliminary toxicity results indicate essentially no mortality for *Ceriodaphnia dubia* after 14 days in the acid rain leachate for each of the four samples. This may be attributed to both the low dissolution of metals and the relatively low toxicity of the constituents.

Ultimately, the fate and bioavailability of engineered nanoparticles in natural aquatic systems are strongly influenced by their ability to remain dispersed in water. Consequently, understanding the colloidal properties of the thermite residues and their particle stability will allow for a more accurate prediction of their environmental, health, and safety effects in aquatic systems. The colloidal stability of engineered nanoparticles depends on their physicochemical properties within a given aqueous medium and is ultimately reflected in the particles' aggregation and deposition behaviour. For this work, the settling kinetics of post-combustion nanothermite residues was determined (Figure 8). Given that the same mass concentration (10 mg L^{-1}) was used for each suspension experiment, the absolute value of the turbidity is directly proportional to *N* for the suspension (Eqn. (2)). Thus, assuming σ_{scat} is equal for all suspensions, then Sample 2 appeared to have the highest initial number density, followed by Sample 3 > Sample 4 >> Sample 1. The difference in particle size is supported by the calculated 1st-order rate constant for settling (k_{set}) as determined by fitting the settling data to a first-order exponential decay. Estimated kinetic parameters (Table 4) show that all particles settled relatively rapidly with the greatest rate of change in *N* observed for Sample 4 followed by Samples 3, 2, and finally 1. These results indicate that the particles have a poor disposition for rewetting. We infer that colloidal stability is limited and if the residual thermite material is exposed to surface water, rapid settling will occur. Thus, the material will most likely be found in sediment and be transport limited.

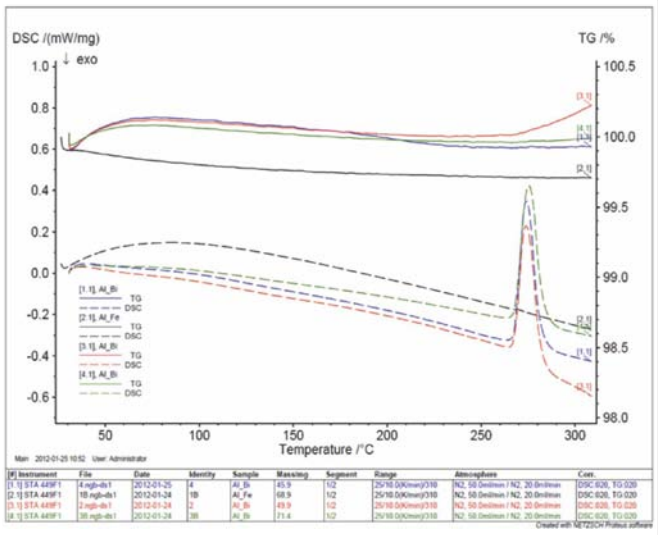

Figure 7: TGA and DSC traces for Samples 1 (blue), 2 (black), 3 (red), and 4 (green). The DSC peak near 270°C corresponds to bismuth melt.

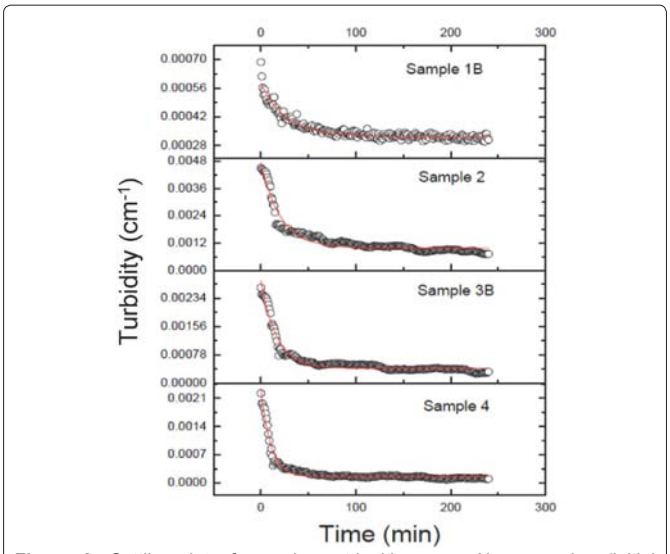

Figure 8: Settling data for each post-ignition nano-Al suspension (initial particle concentrations of 10 mg L^{-1}). The red lines represent the fit from a first-order kinetic equation.

Table 4: Parameter estimates describing the settling behavior of post-ignition nano-aluminum particles, described using a 1st-order kinetic model.*

Sample	$N\sigma_{ext}$ initial (cm^{-1})	$N\sigma_{ext}$ min (cm^{-1})	k_{set}	R^2
1	2.6 x 10^{-4}*	3.2 x 10^{-4}	-0.03687	0.9347
2	3.7 x 10^{-3}	9.8 x 10^{-4}	-0.04823	0.9384
3	2.4 x 10^{-3}	4.0 x 10^{-4}	-0.06057	0.9579
4	2.2 x 10^{-3}	1.6 x 10^{-4}	-0.0971	0.9648

*Note: This model under-predicts the observed $N\sigma_{ext\ initial}$ for Sample 1. Calculations show that for t = 10^{-9} min, $N\sigma_{ext}$ is predicted as = 5.8 x 10^{-4} cm^{-1}.

Conclusions

The studies discussed herein attempt to lay the framework for investigations of the fate and environmental repercussions of nanothermite materials. It is the spent form of the materials, rather than the raw reactants, that ultimately must be disseminated in the environment. To that end, we identified the major chemical constituents of Al/Fe_2O_3 and Al/Bi_2O_3 nanothermite compositions after combustion events and performed preliminary studies that relate the efficacy of transport of these residues in air or water. Ultimately, it was determined that nanothermite residues from expended Al/Fe_2O_3 formulations comprise particles generally larger than 75 μm consisting of a mixture of wuestite and corundum with hercynite, whereas Al/Bi_2O_3 formulations give rise to small (<5 μm) particles consisting of metallic Bi and Al_2O_3. In general, all material products settle quickly in aqueous media and are typically not wettable. Thus, there exists a low potential for water-mediated transport of these materials and limited toxicity of these materials in water. Air transport of the materials is more likely, especially for the smaller-sized products, and so represents an avenue for continued investigations.

Acknowledgments

The use of trade, product, or firm names in this report is for descriptive purposes only and does not imply endorsement by the U.S. Government. The tests described and the resulting data presented herein, unless otherwise noted, were obtained from research conducted under the Environmental Quality Technology Program of the United States Army Corps of Engineers by the USAERDC. Permission was granted by the Chief of Engineers to publish this information. The findings of this report are not to be construed as an official Department of the Army position unless so designated by other authorized documents. The authors also thank Frances Hill and Andrea Scott of the USACE for their editorial comments.

References

1. Miziolek AW (2002) Nanoenergetics: An Emerging Technology Area of National Importance. U.S. Army Research Laboratory / AMPTIAC, Rome, NY, USA.
2. German RM, Ham V (1979) Observations on the compaction of binary thermite powder mixtures. Powder Technol 22: 283-285.
3. Fischer SH, Grubelich MC (1996) A Survey of Combustible Metals, Thermites, and Intermetallics for Pyrotechnic Applications. 32nd AIAA/ASME/SAE/ASEE Joint Propulsion Conference and exhibit, Lake Buena Vista, FL.
4. Hinshaw JC, Blau RJ (1995) Thermite compositions for use as gas generants comprising basic metal carbonates and/or basic metal nitrates. United States Patent No: 5,429,691, Washington, DC, USA.
5. Osborne DT, Pantoya ML (2007) Effect of Al Particle Size on the Thermal Degradation of Al/Teflon Mixtures. Combust Sci Technol 179: 1467-1480.
6. Shoshin YL, Mudryy RS, Dreizin EL (2002) Preparation and characterization of energetic Al-Mg mechanical alloy powders. Combust Flame 128: 259-269.
7. Armstrong R (1990) Models for Gasless Combustion in Layered Materials and Random Media. Combust Sci Technol 71: 155-174.
8. Hao YJ, Tanaka T (1988) Role of the contact points between particles on the reactivity of solids. Can J Chem Eng 66: 761-766.
9. Wang LL, Munir ZA, Maximov YM (1993) Thermite reactions: their utilization in the synthesis and processing of materials. J Mater Sci 28: 3693-3708.
10. Brown ME, Taylor SJ, Tribelhorn MJ (1998) Fuel—Oxidant Particle Contact in Binary Pyrotechnic Reactions. Propellants, Explosives, Pyrotechnics 23: 320-327.
11. Tomasi R, Munir ZA (1999) Effect of Particle Size on the Reaction Wave Propagation in the Combustion Synthesis of Al_2O_3-ZrO_2-Nb Composites. J Am Ceram Soc 82: 1985-1992.
12. Valliappan S, Swiatkiewicz J, Puszynski JA (2005) Reactivity of aluminum nanopowders with metal oxides. Powder Technol 156: 164-169.
13. Wang L, Luss D, Martirosyan KS (2011) The behavior of nanothermite reaction based on Bi_2O_3/Al. J Appl Phy 110: 074311-074311-7.
14. Darlington TK, Neigh AM, Spencer MT, Nguyen OT, Oldenburg SJ (2009) Nanoparticle characteristics affecting environmental fate and transport through soil. Environ Toxicol Chem 28: 1191-1199.
15. Mueller NC, Nowack B (2008) Exposure Modeling of Engineered Nanoparticles in the Environment. Environ Sci Technol 42: 4447-4453.
16. Puszynski J (2009) Processing and characterization of aluminum-based nanothermites. J Therm Anal Calorim 96: 677-685.
17. Bulian CJ, Puszynski JA, Swiatkiewicz JJ (2008) Tunability of Nanoenergetic Materials. Proceedings of Annual AIChE Meeting, Philadelphia, PA.
18. Puszynski JA, Bulian CJ, Swiatkiewicz JJ (2008) Ignition Characteristics of Nanothermite Systems. Int J Energetic Materials Chem Prop 7: 73-86.
19. Novacentrix
20. Accumet Materials Co.
21. Clark Manufacturing LLC
22. Nanostructured & Amorphous Materials, Inc.
23. Puszynski JA, Bichay MM, Swiatkiewicz JJ (2010) Wet Processing and Loading of Percussion Primers Based on Metastable Nanoenergetic Composites, United States Patent No. 7,670,446. Washington, DC.
24. Mackay CE, Johns M, Salatas JH, Bessinger B, Perri M (2006) Stochastic probability modeling to predict the environmental stability of nanoparticles in aqueous suspension. Integr Environ Assess Manag 2: 293-298.
25. Aumann CE, Skofronick GL, Martin JA (1995) Oxidation behavior of aluminum nanopowders. J Vac Sci Technol B 13: 1178-1183.
26. Zhang K, Rossi C, Rodriguez GAA, Tenailleau C, Alphonse P (2007) Development of a nano-Al/CuO based energetic material on silicon substrate. Appl Phys Lett 91: 113117-113117-3.
27. Puszynski JA, Bulian CJ, Swiatkiewicz JJ (2007) Processing and Ignition Characteristics of Aluminum-Bismuth Trioxide Nanothermite System. Journal of Propulsion and Powder 23: 698-706.
28. Trebs A, Foley TJ (2010) Semi-Empirical Model for Reaction Progress in Nanothermite. Journal of Propulsion and Power 26: 772-775.
29. Fitzner K (1979) Thermodynamic properties and cation distribution of the ZnFe2O4-Fe3O4 spinel solid solutions at 900°C. Thermochimica Acta 31: 227-236.
30. Mitchell TE (1999) Dislocations and Mechanical Properties of MgO-Al_2O3 Spinel Single Crystals. J Am Ceram Soc 82: 3305-3316.
31. Serfontein WJ, Mekel R, Bank S, Barbezat G, Novis B (1979) Bismuth toxicity in man - I. Bismuth blood and urine levels in patients after administration of a bismuth protein complex (Bicitropeptide). Res Commun Chem Pathol Pharmacol 26: 383-389.
32. Serfontein WJ, Mekel R (1979) Bismuth toxicity in man II. Review of bismuth blood and urine levels in patients after administration of therapeutic bismuth formulations in relation to the problem of bismuth toxicity in man. Res Commun Chem Pathol Pharmacol 26: 391-411.

33. Fraga CG, Oteiza PI (2002) Iron toxicity and antioxidant nutrients. Toxicology 180: 23-32.

34. Jeng HA, Swanson J (2006) Toxicity of Metal Oxide Nanoparticles in Mammalian Cells. J Environ Sci Health A Tox Hazard Subst Environ Eng 41: 2699-2711.

35. Warheit DB, Brock WJ, Lee KP, Webb TR, Reed KL (2005) Comparative pulmonary toxicity inhalation and instillation studies with different TiO_2 particle formulations: Impact of surface treatments on particle toxicity. Toxicol Sci 88: 514-524.

36. Lam CW, James JT, McCluskey R, Hunter RL (2004) Pulmonary Toxicity of Single-Wall Carbon Nanotubes in Mice 7 and 90 Days After Intratracheal Instillation. Toxicol Sci 77: 126-134.

37. Warheit DB, Laurence BR, Reed KL, Roach DH, Reynolds GA, et al. (2004) Comparative Pulmonary Toxicity Assessment of Single-wall Carbon Nanotubes in Rats. Toxicol Sci 77: 117-125.

38. Karakoti AS, Hench LL, Seal S (2006) The potential toxicity of nanomaterials—The role of surfaces. JOM 58: 77-82.

39. Heyder J (2004) Deposition of Inhaled Particles in the Human Respiratory Tract and Consequences for Regional Targeting in Respiratory Drug Delivery. Proc Am Thorac Soc 1: 315-320.

40. Joner EJ, Hartnik T, Amundsen CE (2008) Environmental fate and ecotoxicity of engineered nanoparticles. Bioforsk Report no. TA 2304/2007.

41. Ju B, Fan T (2009) Experimental study and mathematical model of nanoparticle transport in porous media. Powder Technol 192: 195-202.

42. Aussawasathien D, Teerawattananon C, Vongachariya A (2008) Separation of micron to sub-micron particles from water: Electrospun nylon-6 nanofibrous membranes as pre-filters. J Membr Sci 315: 11-19.

43. Zhang H, Chen B, Banfield JF (2010) Particle Size and pH Effects on Nanoparticle Dissolution. J Phys Chem C 114: 14876-14884.

44. Brown GE, Trainor TP, Chaka AM (2008) Geochemistry of Mineral Surfaces and Factors Affecting Their Chemical Reactivity In: Chemical Bonding at Surfaces and Interfaces (Nilsson A, Pettersson LGM, Norskov JK). Elsevier, Amsterdam 457-509.

Author Affiliations

Top

[1]*Environmental Laboratory, US Army Engineer Research and Development Center, 3909 Halls Ferry Rd., Vicksburg, MS, 39180*
[2]*Geotechnical and Structures Laboratory, US Army Engineer Research and Development Center, 3909 Halls Ferry Rd., Vicksburg, MS, 39180, USA*
[3]*Innovative Materials and Processes LLC, 8420 Blackbird Ct., Rapid City, SD, 57703, USA*